Experimental and numerical evaluation on debonding of fully grouted rockbolt under pull-out loading

Shuisheng Yu
Zhongyuan University of Technology https://orcid.org/0000-0001-9755-8454
Wancheng Zhu (zhuwancheng@mail.neu.edu.cn)
Northeastern University https://orcid.org/0000-0001-9912-2152
Leilei Niu
Northeastern University

Research

Keywords: Fully grouted rockbolt, Debonding, Pull-out load, Ultrasonic guided wave propagation

Posted Date: September 21st, 2021

DOI: https://doi.org/10.21203/rs.3.rs-910522/v1

Experimental and numerical evaluation on debonding of fully grouted rockbolt under pull-out loading

Shuisheng Yu[1,2], Wancheng Zhu[1*], Leilei Niu[1]

[1] Center for Rock Instability and Seismicity Research, Department of Mining Engineering, School of Resource and Civil Engineering, Northeastern University, Shenyang, 110819, China

[2] School of Architectural Engineering, Zhongyuan University of Technology, Zhengzhou, 450007, China

*Corresponding author. *E-mail address*: zhuwancheng@mail.neu.edu.cn (W.C. Zhu)

Abstract: The axial loading in rockbolts changes due to stress redistribution and rheology in the country rock mass. Such a change may lead to debonding at rockbolt to grout interface or rupture of the rockbolt. In this study, based on laboratory experiments, ultrasonic guided wave propagation in fully grouted rockbolt under different pull-out loads was investigated in order to examine the resultant debonding of rockbolt. The signals obtained from the ultrasonic monitoring during the pull-out test were processed using wavelet multi-scale analysis and frequency spectrum analysis, the signal amplitude and the amplitude ratio (Q) of low frequency to high frequency were defined to quantify the debonding of rockbolt. In addition to the laboratory test, numerical simulation on the effect of the embedment lengths on ultrasonic guided wave propagation in rockbolt was conducted by using a damage-based model, and the debonding between rockbolt and cement mortar was numerically examined. It was confirmed that the ultrasonic guided wave propagation in rockbolt was very sensitive to the debonding because of pull-out load, therefore, the critical bond length could be calculated based on the propagation of guided wave in the grouted rockbolt. In time domain, the signal amplitude in rockbolt increased with pull-out load from 0 kN to 100 kN until the completely debonding, thus quantifying the debonding under the different pull-out loads. In the frequency domain, as the Q value increased, the debonding length of rockbolt decreased exponentially. The numerical results confirmed that the guided wave propagation in the fully grouted rockbolt was effective in detecting and quantifying the debonding of rockbolt under pull-out load.

Keywords: Fully grouted rockbolt; Debonding; Pull-out load; Ultrasonic guided wave propagation

1. Introduction

As an important part of the support system, rockbolt is widely used for the reinforcement and support of slopes and roadways (Wang et al. 2009). In geotechnical and mining engineering, it is imperative to use effective and non-destructive scientific methods to test rockbolt bond quality, because rockbolts cannot be observed directly, and deterioration of the surrounding environment can increase the occurrence of rock burst and landslide. For the detection of rockbolt bond quality, Beard and Lowe (2003) and Beard et al. (2003) used numerical simulation methods to determine the wave attenuation at low and high frequencies in the rockbolts, and analyzed the influence on wave attenuation of the elastic modulus, the thickness of the anchorage grout, and the quality of the rockbolt/grout interface. Ivanović and Neilson (2013) studied potential damage in grouted rockbolts and determined the effective bond length. The rockbolt bond integrity could be evaluated using ultrasonic guided wave and hammer impact (Lee et al. 2012; Suits et al. 2008; Yu et al. 2013, 2016). The energy transfer in rockbolt was studied by experimentally and numerically, and the results showed that the length of rockbolts and the thickness of anchorage grout could be determined according to the wave propagation signal received at the free end of the rockbolt (Zima and Rucka 2017). Zima and Rucka (2018) studied the influence of the location of debonding on the wave conversion and diffraction. Zou et al. (2010) analyzed the effects of grout strength and air content in the grout on the rockbolt bond quality, and showed that the guided wave rapidly attenuated with an increase in grout strength, and the group velocity increased with the quantity of the air content. Cui and Zou (2012) studied the attenuation of ultrasonic guided wave in grouted rockbolt using numerical simulation and experimentally confirmed the influence of rockbolt defect and lack of mortar on grouted rockbolt.

Debonding of rockbolt can be detected by analyzing the ultrasonic guided wave propagation in rockbolt, and the difficulty is that the reflected waves at various interfaces exist in a mixed and complex form in the detected signal, the detection signal is observed in the time domain, and is mainly expressed as low-frequency signal, and the high-frequency component is covered (Xiao et al. 2006). Therefore, it is difficult to directly obtain the arrival time of the reflected wave from the actual detection signal and signal processing is required to obtain a reasonable signal. Fourier and

wavelet transform processes have been used for this type of signal analysis (Lee et al.2012; Bouden et al. 2012; Kwun et al. 1998; Chen and Wissawapaisal 2002; Rizzo 2006; Chen and Wilcox 2007; Chaki and Bourse 2009a, 2009b;). Lee et al. (2012) used Fourier and wavelet transform to evaluate rockbolt integrity and concluded that the magnitude of the spectral rate, the energy velocity, and the phase velocity could be used as indicators of integrity. Kwun et al. (1998) investigated the effect of tensile loading on the longitudinal mode elastic wave propagation in seven-wire strands. The results indicated that a certain portion of the frequency components of the wave was highly attenuated and absent in the frequency spectrum of the wave. Chen and Wissawapaisal (2002) reported that the traveling time of the stress wave in the wire strand was affected due to the elongation of the strand and the changes in wave velocities when the strand was subjected to tensile force. Rizzo (2006) conducted experiments on ultrasonic wave propagation in seven-wire strands loaded at different stress levels and reported that the ultrasonic features were sensitive to the variation of applied load. Chen and Wilcox (2007) analyzed the influence of load on guided wave propagation, and found that the guided wave phase velocity increased and the group velocity decreased with increased applied load. The research results of Chaki and Bourse (2009A, 2009B) illustrated the potential and suitability of the guided wave method to evaluate the stress levels in seven-wire steel strands.

With regard to the numerical simulation on the wave propagation in rockbolt, many scholars used idealized ultrasonic guided wave packets as the excitation signal in the numerical simulation of rockbolt detection (Liu et al. 2017; Ni and Iwamoto 2002; Sun et al. 2006; Ren and Li 2009). Liu et al. (2017) analyzed the influence of tensile stress on ultrasonic guided waves propagation in steel cables based on the fast Fourier transform. The results showed increased ultrasonic guided wave energy with increased tensile force. Ren et al. (2009) used wavelet multi-scale analysis to obtain the reflection signal of the rockbolt bottom in the low-frequency component and detail signals in the high-frequency component.

In the above studies, it could be seen that the majority of the past studies were on the non-destructive testing of the bond quality of rockbolt in the absence of external loading using the guided wave technique, this is inconsistent with the fact that the rockbolt is under stress in actual engineering. The mining stress field in the rock mass usually varies due to the on-going mining

operations, leading to the variation of the axial loading in the rockbolt, therefor, it is necessary to detect the debonding length of rockbolt under various pull-out loads to ensure the safety and avoid the accident of grouted rockbolt systems. This study aimed to evaluate the debonding of rockbolt under different pull-out load according to the analysis of ultrasonic guided wave propagation. In this regards, the wavelet multi-scale analysis and frequency spectrum analysis were used for processing the signal obtained from the guided wave propagation. Finally, grouted rockbolt system with different bond lengths was analyzed by numerical simulation, and the debonding under various levels of pull-out loadings was further examined.

2. Guided wave propagation and wavelet transform theory

2.1. Guided wave propagation theory

2.1.1 Guided wave propagation in free rockbolt

Determination of the frequency dependent dispersion curve in ultrasonic guided wave is required for non-destructive testing (Hayashi et al. 2004). The dispersion curve represents the fundamental information of the guided wave propagation: wavelength, phase velocity, and group velocity, which can be expressed by the Pochhammer-Chree frequency dispersion equation of a longitudinal guided wave (Hayashi et al. 2004):

$$\frac{2\alpha}{a}\left(\beta^2+k^2\right)J_1(\alpha a)J_1(\beta a)-\left(\beta^2-k^2\right)^2 J_0(\alpha a)J_1(\beta a)-4k^2\alpha\beta J_1(\alpha a)J_0(\beta a)=0, \tag{1}$$

where $J_n()$ is the n-order first Bessel function. a is the rockbolt diameter, and parameters α and β can be defined as：

$$\alpha^2=\frac{\omega^2}{c_L^2}-k^2, \tag{2}$$

$$\beta^2=\frac{\omega^2}{c_T^2}-k^2, \tag{3}$$

where k is the wave number, ω is the circular frequency, c_L is the longitudinal wave velocity, and c_T is the transverse wave velocity. Namely,

$$c_L=\sqrt{\frac{E(1+\nu)}{\rho(1+\nu)(1-2\nu)}}, \tag{4}$$

115 $$c_T = \sqrt{\frac{E}{2\rho(1+\nu)}}, \quad (5)$$

116 where E is the elastic modulus, ρ is the density, and ν is Poisson's ratio.

117 During guided wave propagation, the guided wave group velocity (c_g) in rockbolt is

118 $$c_g = \frac{d\omega}{dk}. \quad (6)$$

119 According to the material parameters listed in Table 1, the Pochhammer-Chree frequency
120 dispersion equation can be solved to obtain the frequency dispersion curve of the guided wave
121 group velocity in free rockbolt. In the low frequency range, only the guided wave of *L*(0,1) mode
122 appeared, and the guided wave of other modes exhibited a cut-off frequency. Below the cut-off
123 frequency, the guided wave attenuated rapidly and could not propagate any longer, and above the
124 cut-off frequency, the guided wave began to propagate. Therefore, a frequency segment with a
125 single mode was selected to facilitate the signal analysis. As shown in Fig. 1(a), when the
126 frequency was 145 kHz, the guided wave of *L*(0,2) mode appeared, thus adding complexity to the
127 signal analysis. For the free rockbolt, there was only one mode of guided wave with the frequency
128 ranging from 0 to 145 kHz, and it is conducive to signal analysis.

129 [Table 1 goes here]

130 [Fig. 1 goes here]

131 *2.1.2 Guided wave propagation in grouted rockbolt*

132 The Pochhammer-Chree frequency dispersion equation with the parameters listed in Table 2
133 was used to get the frequency dispersion curve of the guided wave group velocity in grouted
134 rockbolt (Fig. 1(b)). Within the frequency range from 0 to 200 kHz, there were eight modes in
135 propagation process of the guided wave. Due to the rapid attenuation of the guided wave energy in
136 the grouted rockbolt, the guided wave frequency decreased. Thus, within the frequency ranging
137 from 0 to 22 kHz, only mode *L*(0,1) existed, and it was conducive to signal analysis.

138 *2.2. Wavelet transform theory*

139 The bond quality and debonding of rockbolt is detected by ultrasonic guided wave, and in its

detection signal, the reflected waves at various interfaces existed in mixed and complex forms. In the time domain, the detection signal is mainly represented by low-frequency signal, while the high-frequency component is covered. It is difficult to obtain the arrival time of reflection waves from the detection signal. To address this issue, the wavelet multi-scale analysis was used to analyze the discrete signal (Ren and Li 2009; Sun et al. 2014). The four scales of db6 wavelet were used to analyze the signal, the rockbolt bottom reflection time could be found in the low-frequency signal (Sun et al. 2014). The bottom reflection signal was obtained in the low-frequency component and the detail signal was obtained in the high-frequency component.

Wavelet transform is a unique time-frequency analysis method that offers multi-resolution or multi-scale analysis by decomposing the signal into different scale space to reflect the different frequency components of the signal (Ren and Li 2009; Sun et al. 2014). By selecting the appropriate scaling factor and moving factor, we can obtain a telescoping window and choose the appropriate wavelet, so that the wavelet transform has the ability to characterize the local characteristics of the signal in both the time and frequency domains.

The wavelet is generated by a function $\psi(t)$ through moving and telescoping and satisfies the condition of $\int_{-\infty}^{+\infty}\psi(t)=0$.

$$\psi_{a,b}(t)=|a|^{-1/2}\psi\left(\frac{t-b}{a}\right),\quad a,b\in R,a\neq 0 \tag{7}$$

where, $\psi(t)$ is the base wavelet or mother wavelet, a is the scaling factor, and b is the moving factor. The function $f(t)$ in $L^2(R)$ is expanded under the wavelet basis, and this expansion is called the wavelet transform of $f(t)$. Its expression is:

$$Wf(a,b)=|a|^{-1/2}\int_{-\infty}^{+\infty}f(t)\psi^*\left(\frac{t-b}{a}\right)dt\,. \tag{8}$$

It can be seen from formula (8), the wavelet transform makes the inner product of the signal to be analyzed and a group of wavelet function clusters, and transforms the time function into the time-scale phase plane to extract some characteristics of the original signal in scale (frequency) and position (time).

Of different methods of wavelet analysis, the Daubechies wavelet series offers good

compactly supported, smoothness, and approximate symmetry. It is widely used to analyze non-stationary signal. Here, we selected db6 as the wavelet basis and performed 5-layer decomposition to obtain the high-frequency and low-frequency components.

3. Test design

3.1. Specimen design

Ribbed rockbolts with 25 mm diameter and 2500 mm length were used and the rock mass that would be reinforced was simulated with a hollow cylinder made of concrete. The diameter and length of the hollow cylinder were 150 and 1500 mm, respectively. The embedment length of rockbolt was 1500 mm. The details of the testing sample preparation were presented in Fig. 2.

[Fig. 2 goes here]

The specimen was a hollow cylinder made of C40 concrete, which consisted of: (1) Ordinary Portland cement with a standard 28-day compressive strength of 42.5 MPa; (2) tap water; (3) natural river sand fine aggregates of diameters from 0.3 to 1.18 mm; and (4) cobblestone coarse aggregates of diameters from 5 to 20 mm mixed at a ratio of 1:0.47:1.3:3.02.

The grout was the cement based mixture which consisted of: (1) Ordinary Portland cement with a standard 28-day compressive strength of 42.5 MPa; (2) tap water; and (3) natural river sand fine aggregates of diameters from 0.3 to 0.6 mm.

Pre-investigation pullout test results showed that rockbolt may fail from the bolt shank when high-strength cement mortar was used to grout rockbolt and hollow cylinder specimen. Therefore, to ensure that debonding occurred before the bolt shank failed the cement mortar was prepared at a mix proportion of cement: water: fine aggregate of 1:1:3.2. The mix proportions of the cement mortar and concrete in the test are listed in Table 2.

[Table 2 goes here]

The procedures of the sample preparation for the pull-out test of the rockbolt were as follows [27]. Firstly, the casting mould was made by placing the plain round bar with a diameter of 40 mm in the center of the cylindrical steel tube. Then the concrete mixture was poured into the mould to form the confining medium followed by be vibrated using a poker vibrator. After 48 h curing of the concrete, the plain round bar and the cylindrical steel tubes were removed. Finally, the

194 rockbolts were grouted in the borehole, and 28 days later pull-out tests were conducted.

195 *3.2. Test procedure*

196 A Pull-out Testing Machine (PTM) was designed and manufactured to conduct the rockbolt
197 pull-out test with monitoring of the stress wave propagation in the rockbolt (Yu et al. 2019). The
198 pull-out load was applied to the rockbolt by a hollow jack with 300 kN loading capacity. The
199 schematic diagram of grouted rockbolt systems was shown in Fig. 2(b). Piezoelectric sensors
200 (TH-GP) and ultrasonic emission source (TH-F) were produced by Xiangtan Tianhong Testing
201 Technology Co., Ltd (China). The emission voltages of the ultrasonic emission source were
202 100-1000 V. The piezoelectric sensor was used as the receiving or excitation sensor which could
203 excite 10-cycles sine wave packets with the main frequency of 22 kHz. An ultrasonic excitation
204 sensor was contacted to the loading end (A-end in Fig. 2(b)) of the rockbolt through a coupling
205 agent (such as Vaseline) to generate the signal that was received at the free end (D-end in Fig. 2(b))
206 of the rockbolt by the receiving sensor.

207 The testing procedure was as follows. First, the grouted rockbolt was maintained without
208 pull-out force. The ultrasonic excitation sensor was used to excite the ultrasonic guided wave at
209 the A-end and the wave was received by the receiving sensor at the D-end. Next, the pull-out load
210 was increased to 100 kN and the above steps were repeated. Finally, the rockbolt was pulled until
211 it was completely debonded from the concrete specimen and the ultrasonic guided wave was
212 tested according to above steps.

213 ## 4. Experimental results and discussion

214 *4.1. Wavelet multi-scale analysis*

215 In the schematic diagram presented in Fig. 2(b), the B-end is the bond front-end and the
216 C-end is the bond back-end. The continuous wavelet transform was used to convert ultrasonic
217 TiAl and ^{40}Cr diffusion bonding interface signals into time-scale domain to evaluate the bonding
218 quality (Luan et al. 2011). Therefore, the multi-scale decomposition of the wavelet transform was
219 used in the paper to evaluate the debonding length. In Fig. 3 the multi-scale decomposition of the
220 wave in the rockbolt under different pull-out loads is shown, where ‘s’ is the original signal, ‘a5’ is

the fifth layer approximated signal, and 'd1-d5' are decomposition signals. Fig. 3(a) shows the wavelet multi-scale decomposition of guided wave signals in rockbolt free of pull-out load, the time ($t_{0\mathrm{kN}}$) required for the first wave front to arrive at the D-end was 0.604 ms. The wave velocity (c_0) in the free rockbolt section was 5100 m/s, thus the guided wave propagation time along the 1 m free length of the rock bolt was calculated according to

$$t_0 = 1/c_0 = 0.196(\mathrm{ms}). \tag{9}$$

The wave velocity in the embedment section of the rockbolt was then calculated as

$$c_{0\mathrm{kN}} = 1.5/(t_{0\mathrm{kN}} - t_0) = 3676(\mathrm{m/s}). \tag{10}$$

The high-frequency signals reflected the details of the guided waves, but the d1 and d2 signals are more chaotic, so d3 signal was selected to pick up the wave arrival time. The time ($t_{0\mathrm{kN\text{-}B}}$) to receive the echo signal from the B-end at the D-end was 1.457 ms. Therefore, the time required to propagate from the D-end to the B-end and then reflect back to the D-end was equal to

$$t_{0\mathrm{kN\text{-}B\text{-}D}} = t_{0\mathrm{kN\text{-}B}} - t_{0\mathrm{kN}} = 0.853(\mathrm{ms}). \tag{11}$$

There was 0.3 m free segment at the D-end, so the bond length could be calculated as

$$L_{0\mathrm{kN}} = \left(\frac{t_{0\mathrm{kN\text{-}B\text{-}D}}}{2} - \frac{0.3}{c_0}\right) c_{0\mathrm{kN}} = 1.35(\mathrm{m}), \tag{12}$$

which was 10% different from the actual bond length of 1.5 m.

The time ($t_{0\mathrm{kN\text{-}A}}$) to receive the echo signal from the A-end at the D-end was 1.764 ms. The time difference between the A-end and B-end echo signals received at the D-end was equal to

$$t_{0\mathrm{kN\text{-}A\text{-}B}} = t_{0\mathrm{kN\text{-}A}} - t_{0\mathrm{kN\text{-}B}} = 0.307(\mathrm{ms}). \tag{13}$$

Thus, the distance from the A-end to the B-end was calculated:

$$L_{0\mathrm{kN\text{-}AB}} = \frac{t_{0\mathrm{kN\text{-}A\text{-}B}}}{2} c_0 = 0.78(\mathrm{m}), \tag{14}$$

which was for 11.4% difference from the actual length of 0.7 m.

Fig. 3(b) presents the wavelet multi-scale decomposition of guided wave signals after completely debonding of rockbolt, the time ($t_{\mathrm{debonding}}$) for the first wave front to arrive at the D-end was 0.572 ms, the wave velocity in the grouted system was calculated as

$$c_{\text{debonding}} = 1.5 \Big/ \left(t_{\text{debonding}} - t_0 \right) = 3989 \left(\text{ms} \right). \tag{15}$$

The time ($t_{\text{debonding-B}}$) to receive the echo signal from the B-end at the D-end was 1.402 ms. Therefore, the time required for the eave to propagate from the D-end to the B-end and then to reflect back to the D-end was equal to:

$$t_{\text{debonding-B-D}} = t_{\text{debonding-B}} - t_{\text{debonding}} = 0.83 \left(\text{ms} \right). \tag{16}$$

Allowing for calculation of the bond length, it was:

$$L_{\text{debonding}} = \left(\frac{t_{\text{debonding-B-D}}}{2} - \frac{0.3}{c_0} \right) c_{\text{debonding}} = 1.42 \left(\text{m} \right), \tag{17}$$

which was for 5.3% difference with the actual bond length of 1.5 m.

The time ($t_{\text{debonding-A}}$) to receive the echo signal from the A-end at the D-end was 1.675 ms. Therefore, the time difference between the A-end and B-end echo signals received at the D-end was:

$$t_{\text{debonding-A-B}} = t_{\text{debonding-A}} - t_{\text{debonding-B}} = 0.273 \left(\text{ms} \right). \tag{18}$$

The distance from the A-end to the B-end was:

$$L_{\text{debonding-AB}} = \frac{t_{\text{debonding-A-B}}}{2} c_0 = 0.696 \left(\text{m} \right), \tag{19}$$

which was for 0.6% difference with the actual length of 0.7 m.

Fig. 3(c) shows the wavelet multi-scale decomposition of guided wave signals under 100 kN of pull-out load, the time (t_{100kN}) of the first wave front to arrive at the D-end was 0.588 ms . The time ($t_{\text{100kN-B}}$) to receive the echo signal from the B-end at the D-end was 1.429 ms. Therefore, the time required to propagate from the D-end to the B-end and then reflect back to the D-end was equal to:

$$t_{\text{100kN-B-D}} = t_{\text{100kN-B}} - t_{\text{100kN}} = 0.841 \left(\text{ms} \right). \tag{20}$$

The pull-out load causes a segment of rockbolt to debond from the concrete. The wave velocity of the grouted rockbolt was 3676 m/s under unloading, and that when the rockbolt completely debonded (as shown in Fig. 3(b)), was 3989 m/s due to the presence of friction between rockbolt and concrete. The initial bond length of rockbolt was 1.5 m, so the debonding

length of the rockbolt from the loading end under 100 kN pull-out load was equal to:

$$L = \frac{c_{\text{debonding}}\left[1.5 - \left(t_{100\text{kN}} - t_0\right)c_{0\text{kN}}\right]}{c_{\text{debonding}} - c_{0\text{kN}}} = 0.752\left(\text{m}\right). \tag{21}$$

But the remaining 0.748 m bond length was still in the bonded state.

The average wave velocity of rockbolt in the grouted system was calculated as $3826\,\text{m/s}$. The time ($t_{100\text{kN-A}}$) to receive the echo signal from the A-end at the D-end was 1.706 ms. Therefore, the time difference between the A-end and B-end echo signals received at the D-end was:

$$t_{100\text{kN-A-B}} = t_{100\text{kN-A}} - t_{100\text{kN-B}} = 0.277\left(\text{ms}\right). \tag{22}$$

The distance from the A-end to the B-end was calculated as

$$L_{100\text{kN-AB}} = \frac{t_{100\text{kN-A}} - t_{100\text{kN-B}}}{2}c_0 = 0.706\left(\text{m}\right), \tag{23}$$

and the difference with the actual length of 0.7 m was 0.9%.

[Fig. 3 goes here]

The comparison between the actual bonding length of rockbolt and that determined by ultrasonic wave is presented in Fig. 4. For the lengths from the A-end to the B-end determined by the ultrasonic wave propagation data, they were 0.78 m, 0.706 m, and 0.696 m, respectively, under 0 kN pull-out load, 100 kN pull-out load, and completely debonding conditions, leading to the relative differences to the actual 0.7 m length of 11.4%, 0.9%, and 0.6%, respectively. Under free and completely debonding condition, the lengths from the B-end to the C-end determined by the ultrasonic wave propagation data were 1.35 m and 1.42m, respectively, resulting in the relative differences with the actual length of 1.5 m of 10% and 5.3%, respectively. However, under 100 kN of pull-out load, the length from the B-end to the C-end could not be determined as it was calculated by back analysis.

[Fig. 4 goes here]

4.2. Spectrum analysis

The frequency of the ultrasonic guided wave signal is significantly important for analyzing the wave propagation in rockbolts. Fourier transform is used to analyze the frequency domain of the received signals. Through the Fourier transform, the signals are decomposed into different

297 spectra. The Fourier transform is the integral of $f(t)$ with respect to *t* ranging from -∞ to +∞.
298 Namely,

299 $$F(\omega)=\int_{-\infty}^{+\infty} f(t)e^{-i\omega t}dt\,, \tag{24}$$

300 where, $f(\omega)$ is the Fourier transform of
301 $f(t)$, i is $\sqrt{-1}$, and the frequency variable ω is the angular
302 frequency.

303 The time domain and frequency domain characteristics of wave propagation in free rockbolt
304 are shown in Fig. 5. In the time domain, due to the influence of various factors (such as the
305 coupling effect between rockbolt and transducer, wires and acquisition module) (Zhang et al.
306 2006), the guided wave energy in free rockbolt dissipated greatly and the amplitude attenuated
307 quickly. In the frequency domain, the main frequency of the guided wave in free rockbolt was 22
308 kHz. Therefore, in the following numerical simulation, an idealized 10-cycles sine wave packets
309 with the main frequency of 22 kHz is input as the excitation signal.

310 [Fig. 5 goes here]

311 [Fig. 6 goes here]

312 Time-frequency analysis has often used to analyze dispersive wave signals (Kishimoto et al.
313 1995; Neild et al. 2003). Fig. 6(a, b) shows the time and frequency domain characteristics of the
314 grouted rockbolt under different pull-out loads. In the time domain, the amplitude of the received
315 signal at the D-end of the rockbolt gradually increased with the pull-out load applied on the
316 rockbolt from 0 kN to 100 kN, until the completely debonding of rockbolt, which indicated
317 maximal energy dissipation because of the good bond condition. In contrast, the amplitude of the
318 received signal was highest when the rockbolt was completely debonded, because the interface
319 bonding between rockbolt and cement mortar was relatively loose, and the energy only was
320 transmitted by the friction, which means that the energy dissipation into the concrete was
321 minimum during wave propagation and thus the bond quality was the worst.

322 It can be seen from the waveform under 0 kN pull-out load, the first received signal in the
323 D-end was severely attenuated and the guided wave packet disappeared. As the pull-out load
324 increased to 100 kN, the debonding developed further and the guided wave packet gradually

appeared due to the weakening energy attenuation.

In the frequency domain, under 0 kN, 100 kN pull-out load, and under completely debonding condition of rockbolt, there were two different frequency bands in the rockbolt, and there was missing frequency band appeared between the these two bands. This was a kind of notch frequency phenomenon, which was observed by Kwun et al. (1998) and Liu et al. (2017). As the pull-out load on the rockbolt increased, the amplitude of the low-frequency part decreased and that of the high-frequency part increased. Under 0 kN pull-out load, at the higher frequency, ultrasonic waves experienced a greater number of interactions with the rockbolt and concrete, which implied higher attenuation (Carrión et al. 2017) and denoted the better bond quality. Therefore, we defined the amplitude ratio (Q) of low frequency (F_{low}) to high frequency (F_{high}), namely $Q = F_{low} / F_{high}$, to quantify rockbolt. The Q values were 6.14, 1.31, and 0.97 under 0 kN, 100 kN pull-out load, and under completely debonding condition, respectively. The relationship between the Q value and the debonding length of rockbolt under various pull-out loads was shown in Fig. 7. As the Q value increased, the debonding length of rockbolt decreased exponentially. This quantitative relation between bonding length and Q value can be use evaluate the bonding length of rockbolts.

[Fig. 7 goes here]

5. Numerical analysis of guided wave propagation in grouted rockbolt

5.1. Numerical model of grouted rockbolt system

The finite element software Abaqus (2014) has often been applied for numerical simulation of the debonding behaviors (Zima and Rucka 2017; Qiao and Chen 2008; Lu and Xu 2013; Chang et al. 2017; Xu et al. 2018; Chen et al. 2011; Henriques et al. 2013, 2015; Yang et al. 2017) and non-destructive testing (Zima and Rucka 2017, 2018) of grouted rockbolt system. In this section, grouted rockbolt system were simulated by four-node bilinear axisymmetric quadrilateral elements with reduced integration (CAX4R) (Fig. 8). The interface at the loaded end of the concrete is fixed during the test for the boundary condition in the rockbolt-grouted system. On the basis of extensive trials, a mesh size of 2 mm for the rockbolt and cement mortar and a mesh size of 5 mm for the concrete are deemed adequate to obtain sufficiently accurate results.

[Fig. 8 goes here]

353 The bond behavior can be modeled by cohesive elements (Qiao and Chen 2008; Lu and Xu
354 2013; Chang et al. 2017; Xu et al. 2018; Park et al. 2015) or surface-based cohesive behavior
355 (Chen et al. 2011; Henriques et al. 2013, 2015; Yang et al. 2017) using traction-separation law in
356 Abaqus. Because the interface thickness is negligibly small, the interface bond behavior between
357 rockbolt (concrete) and cement mortar was modeled by the surface based cohesive behavior in
358 order to reduce the calculation time.

359 [Fig. 9 goes here]

360 The cohesive behavior in the shear directions (Fig. 9) were defined as follows: the linear
361 elastic shear stress-slip relations are defined by the elastic bond stiffness, and damage initiation
362 criteria is met when the maximum bond shear stress is attained, and the damage evolution law for
363 bond is assumed as exponential softening branch (Rezazadeh et al. 2017).

364 The uncoupled constitutive relationship of traction-separation behavior as expressed in
365 Abaqus is as follows (Rezazadeh et al. 2017):

366 $$T=\begin{Bmatrix} t_n \\ t_s \\ t_t \end{Bmatrix}=\begin{bmatrix} k_{nn} & 0 & 0 \\ 0 & k_{ss} & 0 \\ 0 & 0 & k_{tt} \end{bmatrix}\begin{Bmatrix} \delta_n \\ \delta_s \\ \delta_t \end{Bmatrix}=K\delta, \tag{25}$$

367 where t_n is the nominal stress in the normal direction; t_s and t_t are the nominal stresses in the
368 two local shear directions; k_{nn}, k_{ss} and k_{tt} are the corresponding stiffness coefficients; and
369 δ_n, δ_s and δ_t are the corresponding displacements.

370 k_{nn}, k_{ss} and k_{tt} are given by (Lu and Xu 2013):

371 $$k_{ss}=k_{tt}=\tau_m/\delta_m^0, \tag{26}$$

372 $$k_{nn}=100k_{ss}=100k_{tt}, \tag{27}$$

373 where τ_m is the maximum shear strength, and δ_m^0 is the slip value at the maximum shear
374 strength, or the effective displacement at the initiation of damage.

375 The stress components of the traction-separation model are affected by damage.

376 $$t_n=(1-d)\bar{t}_n,\quad t_s=(1-d)\bar{t}_s,\quad t_t=(1-d)\bar{t}_t, \tag{28}$$

377 where $\bar{t}_n$, $\bar{t}_s$ and $\bar{t}_t$ are the stress components predicted by the elastic traction-separation behavior
378 for the current strains without damage. d is the damage variable. For exponential softening,

$$d = 1 - \left\{ \frac{\delta_m^0}{\delta_m^{\max}} \right\} \left\{ 1 - \frac{1 - \exp\left[-\alpha \left(\frac{\delta_m^{\max} - \delta_m^0}{\delta_m^f - \delta_m^0} \right) \right]}{1 - \exp(-\alpha)} \right\}, \quad (29)$$

where δ_m^f is the effective displacement at complete failure. $\delta_m^{\max}$ is the maximum value of the effective displacement attained during the loading history. α is a non-dimensional material parameter that defines the rate of damage evolution.

In the numerical simulation, the input waveform of the ultrasonic guided wave was 10-cycles sine wave packets with the main frequency of 22 kHz obtained by Hanning window (Fig. 10). The comparison between the numerical simulation and the experimental results of the free rockbolt was shown in Fig. 11. The modeled signal received at the other end of rockbolt was in good agreement with the test result, which indicated that the numerical model could reasonably simulate guided wave propagation in rockbolt.

[Fig. 10 goes here]

[Fig. 11 goes here]

5.2. Guided wave propagation in grouted rockbolt with different bond lengths

Numerical simulation on guided wave propagation in grouted rockbolt with different bond lengths (L) of 0.375 m, 0.75 m, 1.125 m, and 1.5 m were conducted, as shown in Fig. 8. Except for the change of bond length, the model dimensions were the same as those for the laboratory test.

5.2.1 The effect of bond length on guided wave propagation in absence of pull-out load

Under 0 kN pull-out load, the guided wave propagation behaviors in grouted rockbolt with different bond lengths was determined as shown in Fig. 12. The waveform was different with that of experiments, because the bonding between the rockbolt and the cement mortar was assumed to be perfect in the numerical simulations. The guided wave had many times of transmission and reflection during propagation in the rockbolt, which resulted in the guided wave energy attenuation and the change of waveforms (Yu et al. 2019). The time required to receive the B-end echo signal at the A-end (positions A, B, C, and D in Fig. 8) became shorter under the increasing bond length. That was, the closer the B-end was to the A-end, the less time required for guided

wave propagated in rockbolt. The guided wave diffracted when it arrived at the B-end. Part of the wave energy reflected from the B-end, part diffracted to the cement mortar and concrete, and the remainder propagated along the rockbolt. For the D-end echo, due to the increased bond length, the distance from the B-end to the A-end became shorter, the guided wave diffracted earlier, because the guided wave energy dissipation increased, the attenuation became faster, the wave velocity decreased, and the time of received echoes was delayed accordingly. When receiving the guided wave signal at the D-end, the guide wave velocity decreased as the bond length increased. The B-end was farther away from the D-end, so the time required to receive the B-end echo signal at the D-end was delayed, as did the time required to receive the A-end echo. The rockbolt bond length could be determined by guided wave propagation time along the rockbolt and the wave velocity.

[Fig. 12 goes here]

5.2.2 The effect of pull-out load on guided wave propagation

The guided wave signals of grouted rockbolt system with bond lengths of 0.375 m, 0.75 m, 1.125 m, and 1.5 m were calculated and are shown in Fig. 13, where the pull-out load was 25 kN. The guided wave propagation is affected by pull-out load. According to the wave propagation theory, the B-end and D-end echo signals could be detected as shown in Fig. 13. The time required to receive the B-end echo at the A-end became shorter as the bond length increased, and the signal fluctuation was more complicated, it indicated that guided wave propagation in the bond rockbolt was sensitive to the pull-out load. The time required to receive the D-end echo prolonged as the bond length increased, because the wave velocity of the guided wave in the bond segment was slower than that in the free rockbolt. Therefore, the longer the bond length is, the slower the guide wave propagating is in the bond segment.

[Fig. 13 goes here]

[Fig. 14 goes here]

Fig. 14 presents the guided wave propagation in the grouted rockbolt system with bond length of 1.5 m under different pull-out loads. When the bond length was the same, the time required to receive the B-end echo signal at the A-end was the same, but the time required to

receive the D-end echo signal at the A-end became shorter as the axial load increased, because the bond state of the rockbolt changed under pull-out load. In this regard, part of rockbolt was debonded or the interface between the rockbolt and the cement mortar was in softening stage (as shown in Fig. 15). The length of debonding or softening around rockbolt increased and the bond quality of rockbolt became worse as the pull-out load increased. The guided wave propagation in the rockbolt was in disorder, because the loading end of the rockbolt was subjected to a large concentrated force, resulting in a strong reflection of the guided wave, which made the received reflection signal extremely complex. The rockbolt was partially debonded from the cement mortar, resulting in a discontinuous interface between the rockbolt and cement mortar that interfered with the guided wave propagation.

[Fig. 15 goes here]

Under the pull-out load of 25 kN, the 0.24 m bond length was in the softening stage (Fig. 15). Axial stress distribution along the rockbolt under 25 kN was determined and shown in Fig. 16: the farther the distance from the B-end, the lower the axial stress. The guided wave had little diffraction when arriving at the B-end, so little energy propagated to the cement mortar and concrete, this was mainly due to the increase of the wave impedance mismatch (the low wave impedance between rockbolt and cement mortar and the high wave impedance betwee rockbolt and air) (Song and Cho 2010).

When the pull-out load was 50 kN, the bond length subjected to 50 kN was 0.46 m (Fig. 15), in which 0.3 m was debonded and 0.16 m was softened. As the pull-out load increased to 100 kN, the debonding length was 0.78 m which was for 3.7% difference with the debonding length of 0.752 m based on the calculated result of wave propagation and 0.176 m was in the softening (Fig.15). At the debonding area, there was a gap between the rockbolt and the cement mortar, the guided wave propagated in the rockbolt and was reflected many times at the debonding area. The propagation velocity of the guided wave in the rockbolt was higher than that in the cement mortar and concrete, guided wave partially dispersed in all directions in the cement mortar and the concrete, so that the attenuation was serious.

[Fig. 16 goes here]

6. Conclusions

In this study, the guided wave propagation in the fully grouted rockbolt under various pull-out loads were experimented and numerically simulated to evaluate the debonding of rockbolt. The following conclusions were obtained:

(1) Based on wavelet multi-scale analysis of guided wave signal, the debonding length of rockbolt under 100 kN load was 0.752 m. In the time domain, the signal amplitude increased with load from 0 kN to 100 kN and until completely debonding of rockbolt, indicating maximum ultrasonic guided wave energy dissipation and best rockbolt bond quality when the rockbolt is free from loading. The energy dissipation was minimum when the rockbolt debonded completely, suggesting the worst bond quality and the largest debonding length.

(2) In the frequency domain, two different frequency bands were found in rockbolt, the amplitude of the high-frequency part increased and that of the low-frequency part decreased as the pull-out load on the rockbolt increased. The amplitude ratio (Q) were 6.14, 1.31, and 0.97 under 0 kN, 100 kN, and completely debonding condition, respectively. As the Q value increased, the debonding length of rockbolt decreased exponentially, and vice versa.

(3) The guided wave propagation in rockbolt was very sensitive to pull-out loads. For the same bond length, under increasing pull-out load, numerical results denoted that the debonding developed gradually before the completely debonding, so did the softening of the interface between rockbolt and cement mortar. The wave impedance mismatch (the low wave impedance between rockbolt and cement mortar and the high wave impedance between rockbolt and air) increased, suggesting the longer debonding of the rockbolt.

The guided wave propagation in the rockbolt systems is very complex because the wave propagation and reflection at various interfaces exist in a mixed and complex form. This study provided basic understanding of quantifying the debonding length based on analysis of the guided wave propagation in the rockbolt system under pull-out load. In the long run, the analysis on the complex waveform should be conducted, in order to effectively non-destructively quantify the bond quality of rockbolt.

Acknowledgment

This work is funded by the National Science Foundation of China (Grant Nos. U1906208, 52104157, and 51874069), and the Fundamental Research Funds for the Central Universities of China (Grant Nos. N180115009 and N180101028). These supports are gratefully acknowledged. The authors thank Mr. Penghui Kang and Mr. Shichang Zhou for their assistance during the laboratory test.

Conflict of Interest

We declare that there is not conflict of Interest.

References

Beard MD, Lowe MJS (2003) Non-destructive testing of rock bolts using guided ultrasonic waves, Int. J. Rock Mech. Min. Sci. 40(4), 527-536.

Beard MD, Lowe MJS, Cawley P (2003) Ultrasonic Guided Waves for Inspection of Grouted Tendons and Bolts, J. Mater. Civ. Eng. 15(3), 212-218.

Bouden T, Nibouche M, Djerfi F et al (2012) Improving Wavelet Transform for the Impact-Echo Method of Non Destructive Testing, Lect. Not. Elect. Eng. 141, 241-247.

Carrión A, Genovés V, Gosálbez J et al (2017) Ultrasonic signal modality: A novel approach for concrete damage evaluation, Cem. Concr. Res. 101, 25-32.

Chaki S, Bourse G (2009a) Guided ultrasonic waves for non-destructive monitoring of the stress levels in prestressed steel strands, Ultrason. 49(2), 162-171.

Chaki S, Bourse G (2009b) Stress Level Measurement in Prestressed Steel Strands Using Acoustoelastic Effect, Exp. Mech. 49(5), 673.

Chang X, Wang G, Liang Z et al (2017) Study on grout cracking and interface debonding of rockbolt grouted system, Constr. Build. Mater. 135, 665-673.

Chen F, Wilcox PD (2007) The effect of load on guided wave propagation, Ultrason. 47(1), 111-122.

Chen GM, Teng JG, Chen JF (2011) Finite Element Modeling of Intermediate Crack Debonding in FRP-Plated RC Beams, J. Compos. Constr. 15(3), 339-353.

514 Chen HL, Wissawapaisal K (2002) Application of Wigner-Ville Transform to Evaluate Tensile
515 Forces in Seven-Wire Prestressing Strands, J. Exp. Mech. 128(11), 1206-1214.
516 Cui Y, Zou DH (2012) Assessing the effects of insufficient rebar and missing grout in grouted rock
517 bolts using guided ultrasonic waves, J. Appl. Geophys. 79, 64-70.
518 Dassault Systemes Simulia (2014） ABAQUS theory manual and users manuals version 6.11.
519 USA.
520 Hayashi T, Song WJ, Rose JL (2004) Guided wave dispersion curves for a bar with an arbitrary
521 cross-section, a rod and rail example, Ultrason. 41(3), 175-183.
522 Henriques J, Gentili F, Silva LSD et al (2015) Component based design model for composite beam
523 to reinforced concrete wall moment-resistant joints, Eng. Struct. 87, 86-104.
524 Henriques J, Silva LSD, Valente IB (2013) Numerical modeling of composite beam to reinforced
525 concrete wall joints : Part I: Calibration of joint components, Eng. Struct. 52(9) , 747-761.
526 Ivanović A, Neilson RD (2013) Non-destructive testing of rock bolts for estimating total bolt
527 length, Int. J. Rock Mech. Min. Sci. 64(12), 36-43.
528 Kishimoto K, Inoue H, Hamada M et al (1995) Time Frequency Analysis of Dispersive Waves by
529 Means of Wavelet Transform, Trans. J. Appl. Mech. 62(4), 841-846.
530 Kwun H, Bartels KA, Hanley JJ (1998) Effects of tensile loading on the properties of elastic-wave
531 propagation in a strand, J. Acoust. Soc. Am. 103(6), 3370-3375.
532 Lee IM, Han SI, Kim HJ et al (2012) Evaluation of rock bolt integrity using Fourier and wavelet
533 transforms, Tunn. Undergr. Space Technol. 28(28), 304-314.
534 Liu X, Wu B, Qin F et al (2017) Observation of ultrasonic guided wave propagation behaviours in
535 pre-stressed multi-wire structures, Ultrason. 73, 196-205.
536 Lu Z, Xu Q (2013) Cohesive zone modeling for viscoplastic behavior at finite deformations,
537 Compos. Sci. Technol. 74(4), 173-178.
538 Luan YL, Sun T, Feng JC et al (2011) Ultrasonic evaluation of TiAl and ^{40}Cr diffusion bonding
539 quality based on time-scale characteristics extraction, NDT & E Int. 44(8), 789-796.
540 Neild SA, Mcfadden PD, Williams MS (2003) A review of time-frequency methods for structural
541 vibration analysis, Eng. Struct. 25(6), 713-728.
542 Ni QQ, Iwamoto M (2002) Wavelet transform of acoustic emission signals in failure of model

composites, Eng. Fract. Mech. 69(6), 717-728.

Park K, Ha K, Choi H et al (2015) Prediction of interfacial fracture between concrete and fiber reinforced polymer (FRP) by using cohesive zone modeling, Cem. Concr. Compos. 63, 122-131.

Qiao PZ, Chen Y (2008) Cohesive fracture simulation and failure modes of FRP–concrete bonded interfaces, Theor. Appl. Fract. Mech. 49(2), 213-225.

Ren ZM, Li Y (2009) Analysis of detection signal and realization on evaluation system of bolt anchoring quality based on sound wave testing, J. Chin. Coal Soc. 36(Supp.1), 191-196. (in Chinese)

Rezazadeh M, Carvelli V, Veljkovic A (2017) Modelling bond of GFRP rebar and concrete, Constr. Build. Mater. 153, 102-116.

Rizzo P (2006) Ultrasonic Wave Propagation in Progressively Loaded Multi-Wire Strands, Exp. Mech. 46(3), 297-306.

Song KI, Cho GC (2010) Numerical study on the evaluation of tunnel shotcrete using the impact-echo method coupled with Fourier transform and short-time Fourier transform, Int. J. Rock Mech. Min. Sci. 47, 1274-1288.

Suits LD, Sheahan TC, Han SI et al (2008) Evaluation of Rock Bolt Integrity using Guided Ultrasonic Waves, Geotech. Test. J. 32(1), 31-38.

Sun B, Zheng XT, Zeng S et al (2014) Multi-scale analysis on anchoring defects diagnosis under multiple measuring points, J. Chin. Coal Soc. 39(7),1385-1390. (in Chinese)

Sun KH, Hong JC, Kim YY (2006) Dispersion-based continuous wavelet transform for the analysis of elastic waves, J. Mech. Sci. Technol. 20(12), 2147-2158.

Wang C, He W, Ning J (2009) Propagation properties of guided wave in the anchorage structure of rock bolts, J. Appl. Geophys. 69(3), 131-139.

Xiao GQ, Liu TY, Zhou LM et al (2006) Application of Multi-resolution analysis in detection of rock anchor bar quality using elastic wave non-detructive method, J. Yangtze River Sci. Res. Ins. 23(4), 67-70. (in chinese)

Xu C, Li Z, Wang S et al (2018) Pullout Performances of Grouted Rockbolt Systems with Bond Defects, Rock Mech. Rock Eng. 51(3), 861-871.

572 Yang WR, He XJ, Dai L (2017) Damage behaviour of concrete beams reinforced with GFRP bars,
573 Compos. Struct. 161, 173-186.
574 Yu JD, Bae MH, Lee I.M et al (2013) Nongrouted Ratio Evaluation of Rock Bolts by Reflection of
575 Guided Ultrasonic Waves, J. Geotech. Geoenviron. Eng. 139, 298-307.
576 Yu JD, Hong YH, Byun YH et al (2016) Non-destructive evaluation of the grouted ratio of a pipe
577 roof support system in tunneling, Tunn. Undergr. Space Technol. 56 (2016) 1-11.
578 Yu SS, Zhu WC, Niu LL et al (2019) Experimental and numerical analysis of fully-grouted long
579 rockbolt load-transfer behavior, Tunn. Undergr. Space Technol. 85, 56-66.
580 Yu T, Chaix JF, Audibert L et al (2019) Simulations of ultrasonic wave propagation in concrete
581 based on a two-dimensional numerical model validated analytically and experimentally,
582 Ultrason. 92, 21-34.
583 Zhang C, Zou DH, Madenga V (2006) Numerical simulation of wave propagation in grouted rock bolts
584 and the effects of mesh density and wave frequency, Int. J. Rock Mech. Min. Sci. 43, 634-639.
585 Zima B, Rucka M (2017) Non-destructive inspection of ground anchors using guided wave
586 propagation, Int. J. Rock Mech. Min. Sci. 94, 90-102.
587 Zima B, Rucka M (2018) Guided ultrasonic waves for detection of debonding in bars partially
588 embedded in grout, Constr. Build. Mater. 168, 124-142.
589 Zou DHS, Cheng J, Yue R (2010) Grout quality and its impact on guided ultrasonic waves in
590 grouted rock bolts, J. Appl. Geophys. 72(2), 102-106.
591

592 # List of table

595

596 Table.1 Material properties of the rockbolt, concrete and cement mortar

Ingredient	Density（kg/m^3）	Elastic modulus（GPa）	Poisson's ratio
Rockbolt	7850	210	0.3
Cement mortar	2100	20	0.19
Concrete	2300	33	0.23

597
598

599 Table. 2 Mix proportions of concrete and cement mortar in test

Ingredient	Water	Cement	Sand	Stone
Concrete	0.47	1	1.3	3.02
Cement mortar	1	1	3.2	0

600

Figures

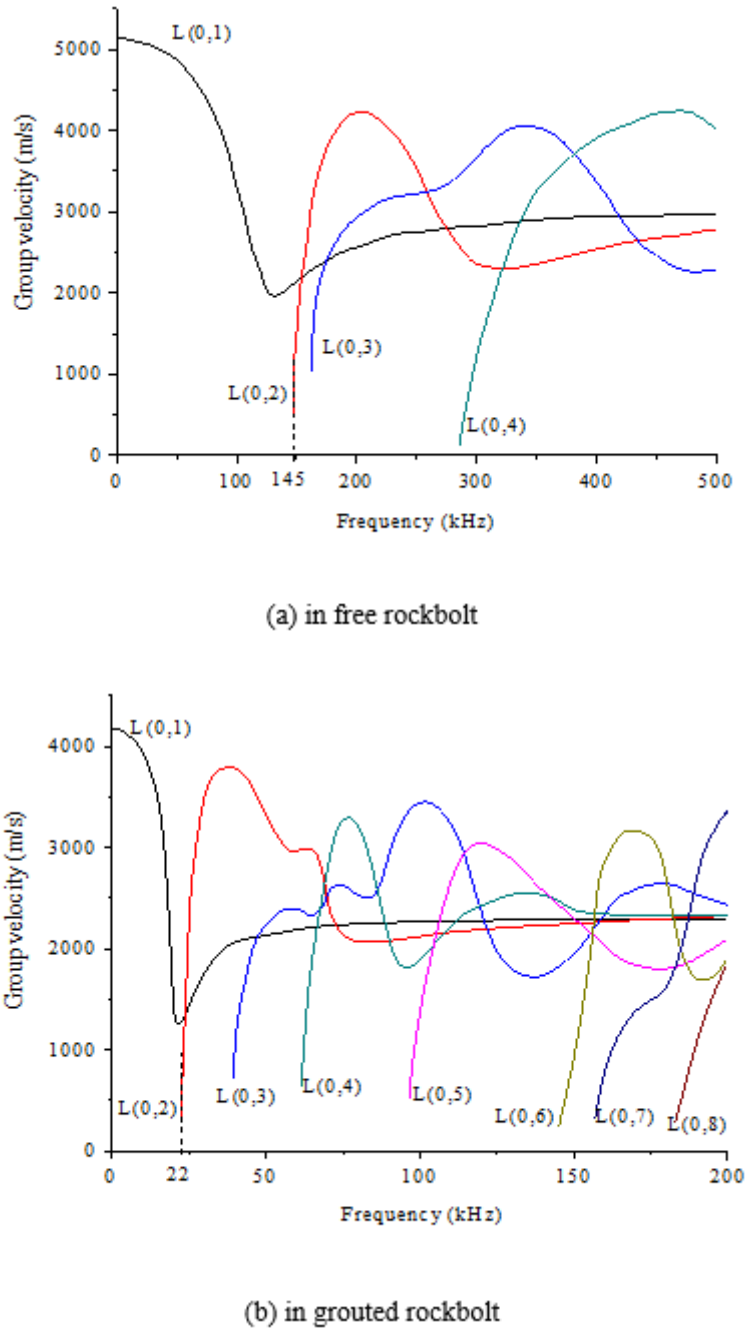

Figure 1

Frequency dispersion curves of group velocity of guided wave in rockbolt

(a) Photograph of rockbolt specimen

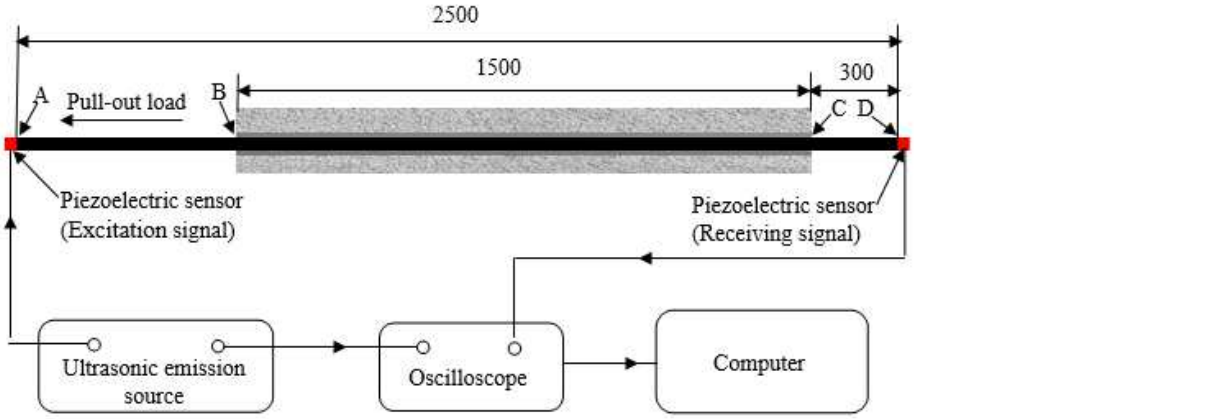

(b) Schematic diagram of experimental system

Figure 2

The schematic diagram for detection of guided wave propagation in grouted rockbolt system (unit: mm)

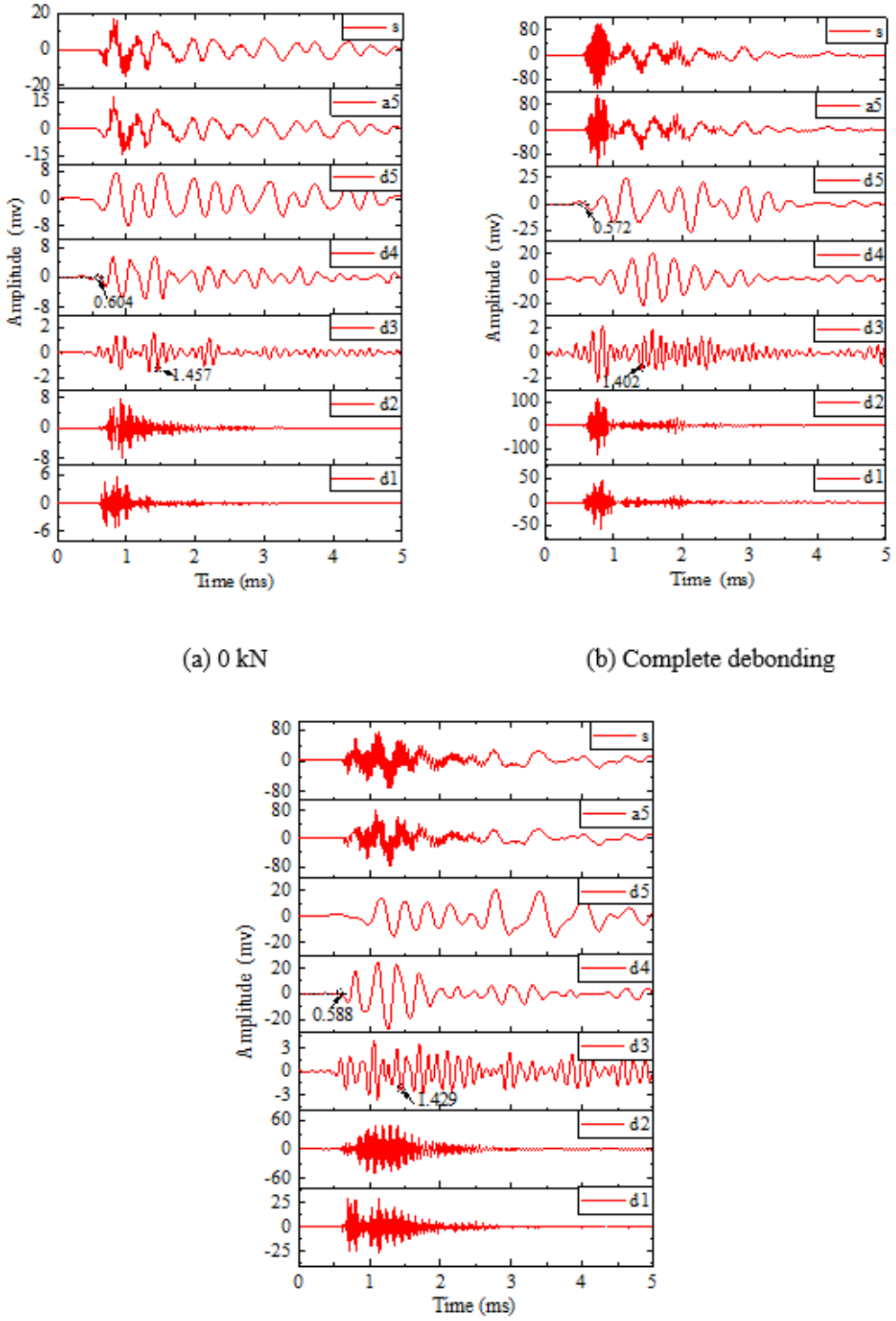

Figure 3

Wavelet multi-scale decomposition of guided wave signals in rockbolt under different pull-out loads

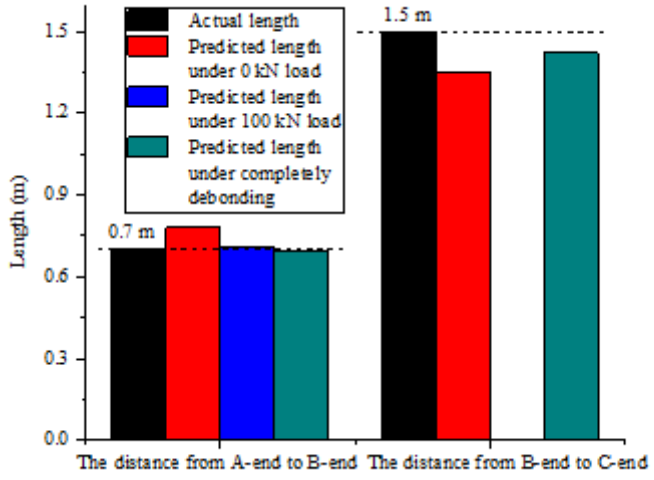

Figure 4

The comparison between actual bond length and the length obtained based on wave propagation analysis

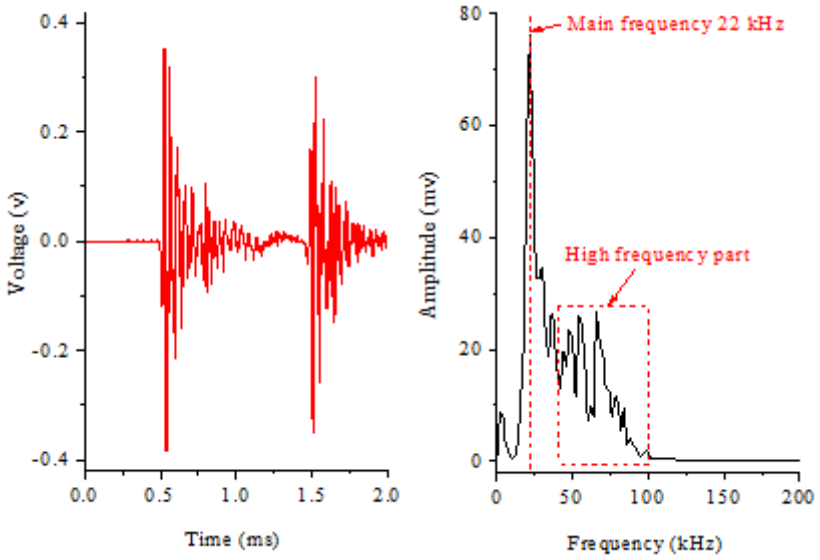

Figure 5

Time domain and frequency domain characteristics in free rockbolt

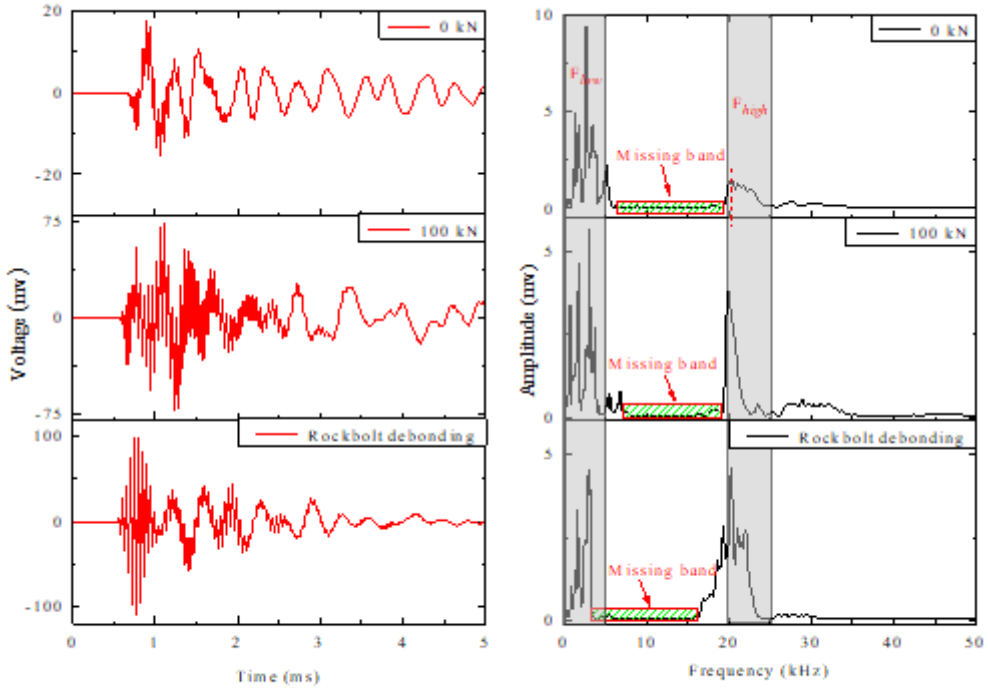

(a) Time domain (b) Frequency domain

Figure 6

Time domain and frequency domain characteristics in grouted rockbolt under different pull-out loads

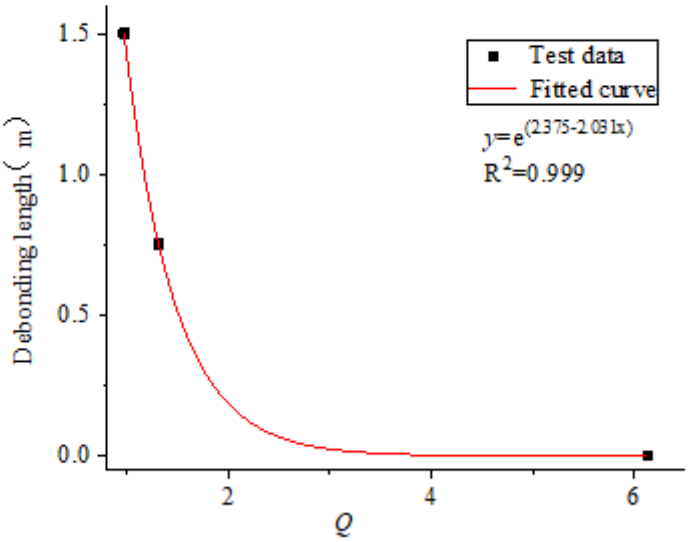

Figure 7

The relationship between the Q value and the debonding length of rockbolt under different pull-out loads

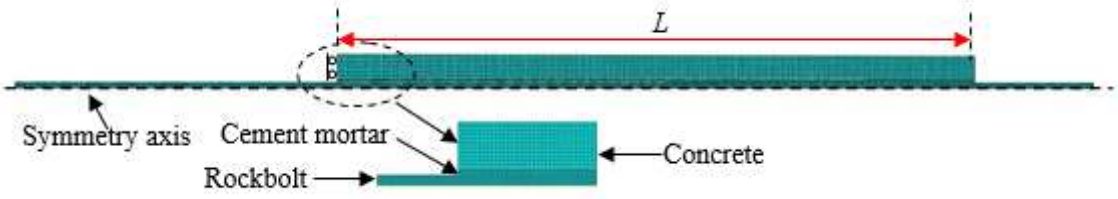

Figure 8

Model setup for the grouted rockbolt systems

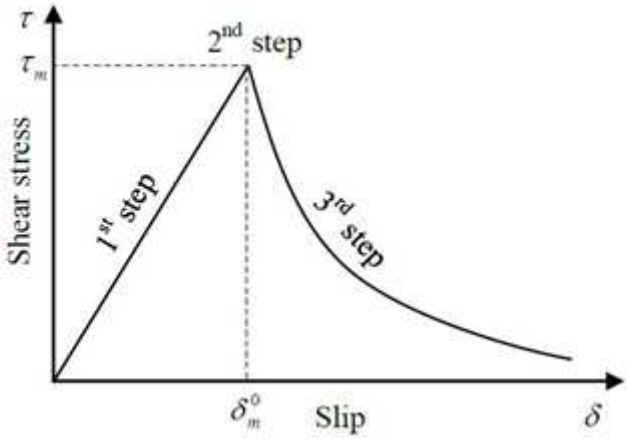

Figure 9

Damage law for the cohesive behavior (Rezazadeh et al. 2017)

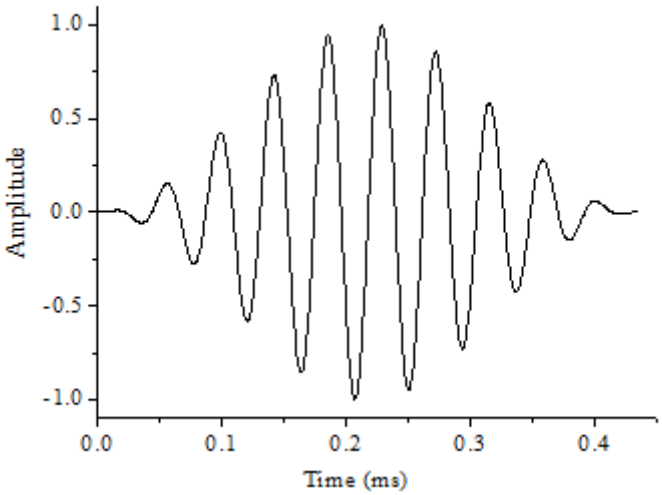

Figure 10

Excitation signal input for the numerical simulation

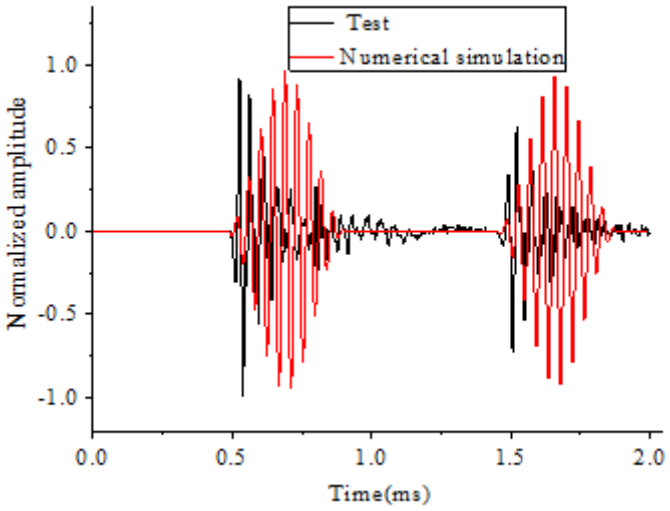

Figure 11

Comparison of numerical and test results of wave propagation in free rockbolt

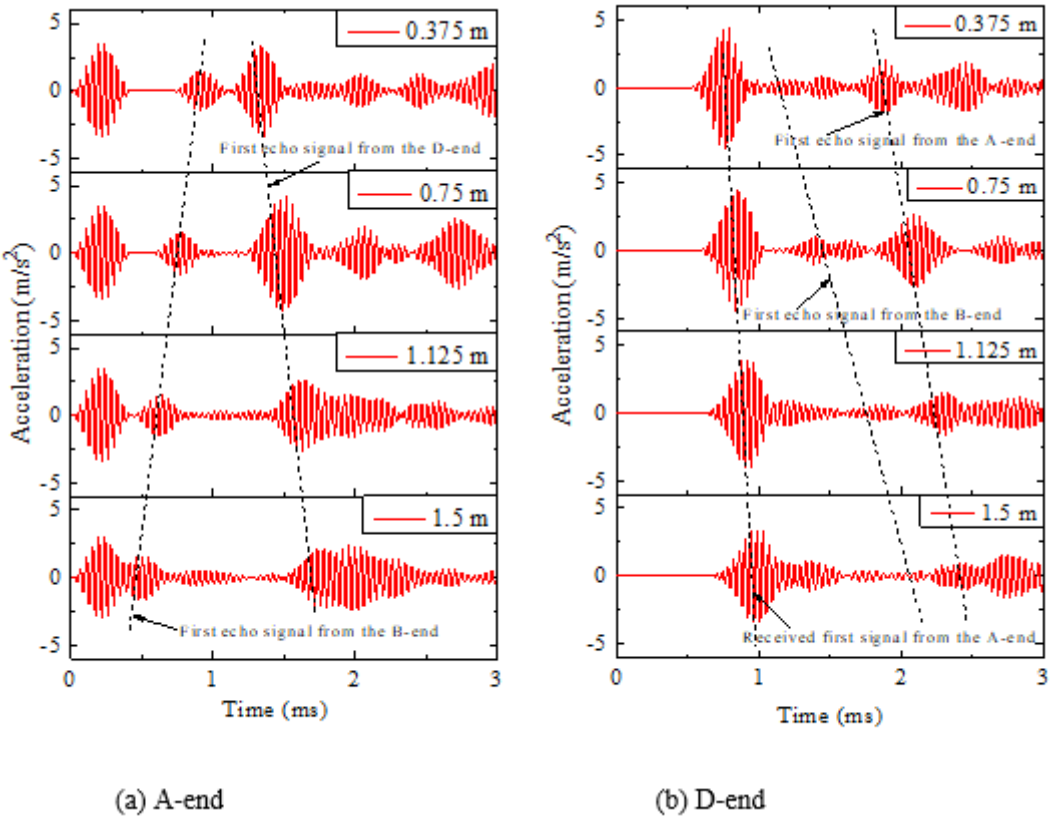

Figure 12

The wave propagation in grouted rockbolt systems with different bond lengths

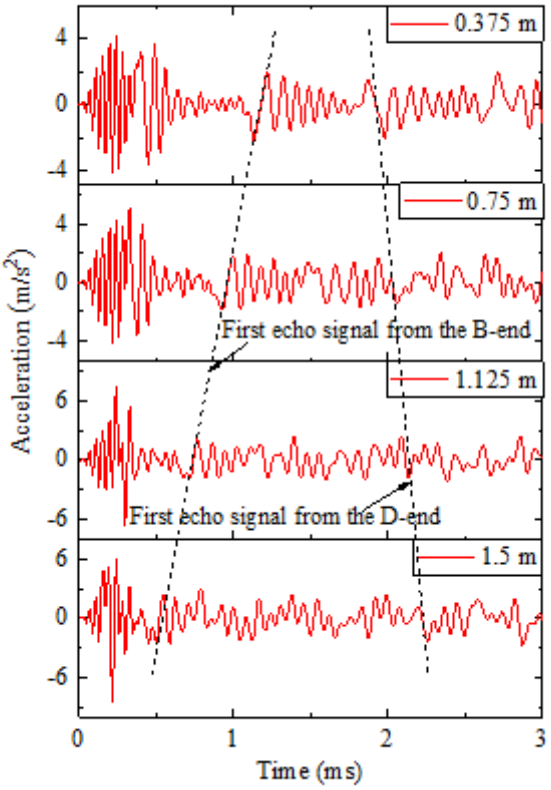

Figure 13

The wave propagation signals with different bond lengths under 25 kN pull-out load

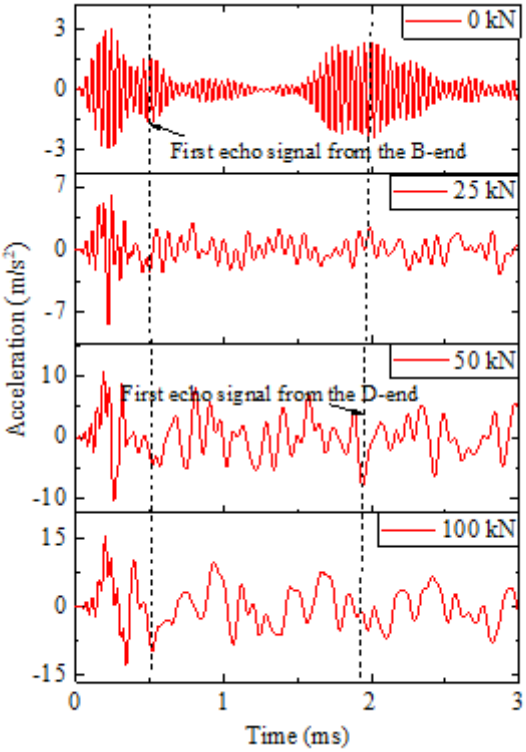

Figure 14

The wave propagation signal with different bond length under different pull-out loads

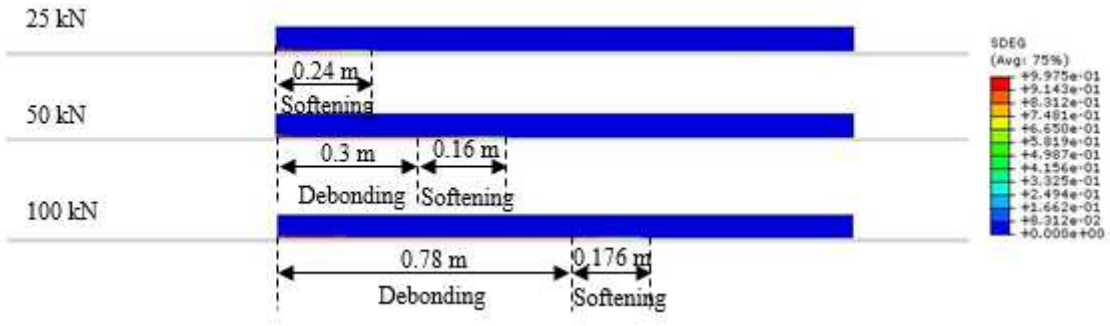

Figure 15

Debonding and softening around rockbolt under different load level (SDEG, Scalar Stiffness Degradation)

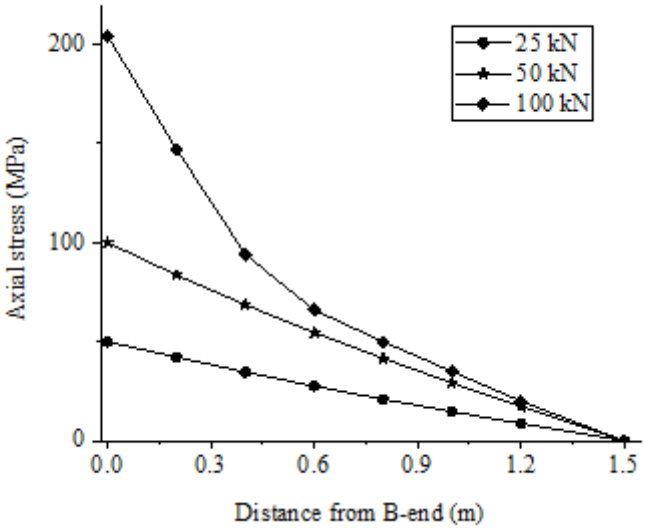

Figure 16

Axial stress distribution along rockbolt under various pull-out loads (with 1.5 m bond length)